Measuring Frequency Fluctuations in Nonlinear Nanomechanical Resonators

Olivier Maillet,[†] Xin Zhou,[†,#] Rasul R. Gazizulin,[†] Rob Ilic,[§] Jeevak M. Parpia,[⊥] Olivier Bourgeois,[†] Andrew D. Fefferman,[†] and Eddy Collin*,[†] [ID]

[†]Université Grenoble Alpes, CNRS Institut Néel, BP 166, 38042 Grenoble Cedex 9, France

[§]Center for Nanoscale Science and Technology, National Institute of Standards and Technology, Gaithersburg, Maryland 20899, United States

[⊥]Department of Physics, Cornell University, Ithaca, New York 14853, United States

ABSTRACT: Advances in nanomechanics within recent years have demonstrated an always expanding range of devices, from top-down structures to appealing bottom-up MoS_2 and graphene membranes, used for both sensing and component-oriented applications. One of the main concerns in all of these devices is frequency noise, which ultimately limits their applicability. This issue has attracted a lot of attention recently, and the origin of this noise remains elusive to date. In this article we present a very simple technique to measure frequency noise in nonlinear mechanical devices, based on the presence of bistability. It is illustrated on silicon-nitride high-stress doubly clamped beams, in a cryogenic environment. We report on the same

T/f dependence of the frequency noise power spectra as reported in the literature. But we also find unexpected *damping fluctuations*, amplified in the vicinity of the bifurcation points; this effect is clearly distinct from already reported nonlinear dephasing and poses a fundamental limit on the measurement of bifurcation frequencies. The technique is further applied to the measurement of frequency noise as a function of mode number, within the same device. The relative frequency noise for the fundamental flexure $\delta f/f_0$ lies in the range 0.5−0.01 ppm (consistent with the literature for cryogenic MHz devices) and decreases with mode number in the range studied. The technique can be applied to *any type* of nanomechanical structure, enabling progress toward the understanding of intrinsic sources of noise in these devices.

KEYWORDS: *nanomechanics, nonlinearity, bifurcation, frequency fluctuations, damping fluctuations*
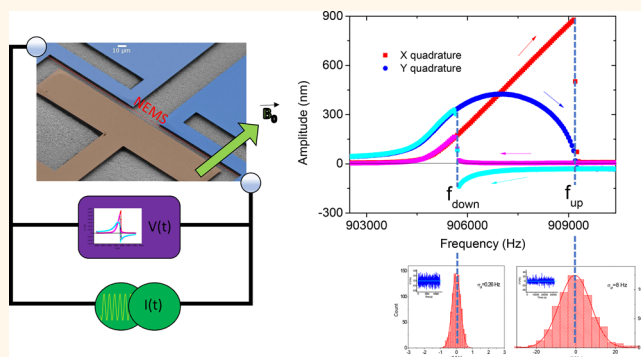
W ithin the past decade nano-electro-mechanical systems (NEMS) have developed with a broad range of applications extending from physics to engineering. In the first place, their size makes them very sensitive transducers of force.[1,2] This had been demonstrated, for example, in the seminal work of D. Rugar *et al.*, in which a cantilever loaded by a magnetic tip reached a detection sensitivity corresponding to the force exerted by a single electronic spin at a distance of about 100 nm.[3] More recently, NEMS have been applied to the detection of small quantities of matter (mass spectroscopy), with precision reaching the single proton.[4] Nowadays, even the quantum nature of the mechanical degree of freedom is exploited for quantum information processing.[5]

In all applications, the quality of the device is intrinsically linked to its level of displayed noise.[6] Specifically, frequency noise in NEMS appears to be a key limiting parameter whose physical origin is still unknown.[7] Besides, only few quantitative experimental studies are available in the literature,[7−10]

especially at low temperatures.[11] The nonlinear frequency noise reported for carbon-based systems[12] is one of the most striking results, revealing the complex nature that the underlying mechanisms can possess.

Frequency noise (or phase noise[6,9,11]) can be understood in terms of *pure dephasing*,[12] making an analogy with nuclear magnetic resonance (NMR), and its impact on a mechanical resonance can be modeled experimentally by means of engineered frequency fluctuations.[13] The physical origin of intrinsic frequency noise is indeed still elusive, since all identified mechanisms studied explicitly display much weaker contributions than the reported experimental values: adsorption−desorption/mobility of surface atoms,[14] experimentally modeled under a Xe flow,[15] or the nonlinear transduction of Brownian motion.[16,17] These efforts in understanding the

microscopic mechanisms at work in mechanical dephasing are accompanied by theoretical support. The nonlinear dephasing/damping has been proposed to originate in nonlinear phononic interactions between the low-frequency mechanical modes and thermal phonons.[18] Finally, a common speculation reported in the literature is that frequency noise is related to defects,[6,11,19] which can be either extrinsic or constitutive of the material (like in a glass). The presence of these so-called two-level systems (TLS) is also proposed to explain damping mechanisms in NEMS,[21,22] and they have been shown recently to lead to peculiar features (especially in the noise) for mesoscopic systems such as quantum bits and NEMS.[20]

Properly measuring frequency noise is not easy; a neat technique presented in the literature relies on cross-correlations present in the two signals of a dual-tone scheme.[7] Moreover, in the spectral domain dephasing and damping are mixed.[12,13,23] In order to separate the contributions, one has to use *both* spectral-domain and time-domain measurements.[12,13] All of these techniques may not be well suited for large-amplitude signals (especially when the system becomes bistable), preventing the exploration of the nonlinear range where nonlinear damping/dephasing may dominate.

In this article we present a method based on bifurcation enabling a very simple measurement of frequency noise in nonlinear bistable resonators. Building on this method, we characterize the intrinsic frequency noise of high-stress silicon nitride (SiN) doubly clamped beams in a cryogenic environment (from 1.4 to 30 K). In particular, we study the three first symmetric modes (n = 1, 3, 5) of one of our devices and demonstrate the compatibility of our results with existing literature. The temperature dependence is indeed similar to ref 11, but we find an unexpected *damping noise*, which is amplified through the bifurcation measurement. This result is distinct from the reported nonlinear phase noise of ref 12, in which the device was *not* bistable. The phenomenon seems to be generic, and we discuss it in the framework of the TLS model. Note that our results demonstrate the existence of an ultimate limit to the frequency resolution of bifurcation points in nonlinear mechanical systems.

RESULTS AND DISCUSSION

A typical doubly clamped NEMS device used in our work is shown in Figure 1. It consists of a 100 nm thick SiN device covered with 30 nm of Al. The width of the beam is 300 nm, and the length L = 250 μm. Another similar sample of L = 15 μm has been characterized. The beams store about 1 GPa of tensile stress, and we define A to be their rectangular cross-section. For fabrication details see Methods below. The device is placed in a ^{4}He cryostat with temperature T_0 regulated between 1.4 and 30 K, under cryogenic vacuum of $\leq 10^{-6}$ mbar. The motion of the beam is driven and detected by means of the magnetomotive scheme.[24,25] For experimental details see Methods below.

A Laplace force $F(t) = F_0 \cos(2\pi f t)$ with $F_0 \propto I_0 L B_0$ is created with a static in-plane magnetic field B_0 and an ac current I_0 fed into the metallic layer (Figure 1). Fields B_0 on the order of 1 T and currents I_0 up to 0.5 μA have been used. The detected signal is the induced voltage $V(t)$ proportional to velocity. It is measured with a lock-in from which we can obtain the two quadratures X, Y of the motion. We call $R = \sqrt{X^2 + Y^2}$ the amplitude of the motion (at a given frequency), defined in meters peak. For all the T_0 and B_0
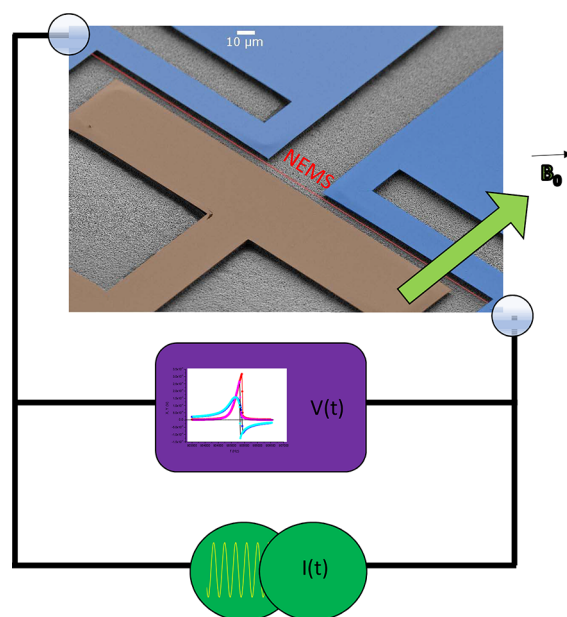

Figure 1. Device and setup. SEM image of the 250 μm device measured in this work. The gate electrode (brown) is not used here. The actual NEMS device is the red-colored string in between the two (light blue) electrodes. The lock-in detector (violet), magnetic field, and drive generator (in green) are also depicted in a schematic fashion to illustrate the magnetomotive technique.

settings used in the present work, the Al layer was not superconducting. A key feature of the magnetomotive scheme is that it enables the ability to tune the Q factor of the detected resonances:[24] this is the so-called *loading* effect.

At low drives, in the linear regime, the quality factor of the resonance $Q = f_0/\Delta f$ is defined from the line width Δf and the resonance frequency f_0 of the mode under study. We consider here only high-Q resonances $Q \gg 1$. In this limit, the X peak is a simple Lorentzian, whose full-width at half-height gives Δf. For large excitation forces, our doubly clamped beams' mechanical modes behave as almost ideal Duffing resonators.[26,27] A typical Duffing resonance is shown in Figure 2. The maximum of the resonance shifts with motion amplitude as $f_{max} = f_0 + \beta R_{max}^2$. β is the so-called Duffing parameter. We assume $\beta > 0$, but the case $\beta < 0$ is straightforward to adapt. R_{max} is the maximum amplitude of motion; it always satisfies $R_{max} = F_0 Q/k_0$ with very good accuracy.[28] k_0 is the mode's spring constant with $f_0 = \frac{1}{2\pi}\sqrt{k_0/m_0}$ and m_0 the mode mass. In the nonlinear Duffing regime, a damping parameter Δf can still be defined from the Q factor deduced from the peak height R_{max}. When frequency noise is negligible, the so-called decoherence time $T_2 = 1/(\pi \Delta f)$ defined from such frequency-domain measurements is just equal to T_1, the relaxation time of the amplitude R in the time domain.[13]

When $R_{max} \geq \frac{2}{\sqrt{3}}R_s$ a response hysteresis opens[29] (see Figure 2). The point in the (R, f) space at which this begins is called the *spinodal point*, with $R_s = \frac{1}{3^{1/4}}\sqrt{\frac{\Delta f}{\beta}}$. Beyond this point, two stable states coexist in a range of frequencies, with the system jumping from one to the other at f_{up} (in an upward frequency sweep) and f_{down} (for downward). These are the two *bifurcation points*. The maximum amplitude of the resonance is reached only on the upper branch. These frequencies are written explicitly:
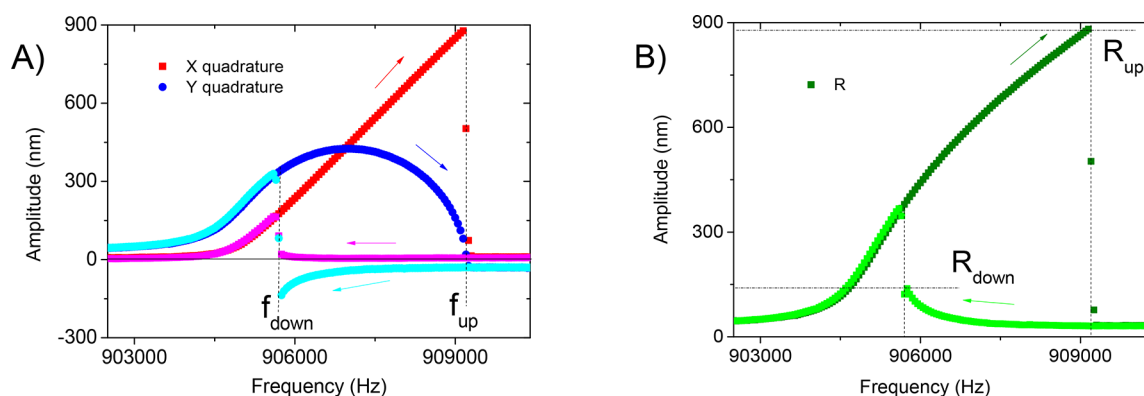
Figure 2. Nonlinear (Duffing) resonance. (A) Duffing resonance line (X and Y quadratures) measured on the 250 μm device at 4.2 K under vacuum, for a drive force of 81 pN, in a 1 T field. The directions of frequency sweeps are depicted by arrows. Vertical dashed lines indicate the two bifurcation points $f_{\text{up,down}}$. (B) Amplitude $R = \sqrt{X^2 + Y^2}$ corresponding to A. Bifurcation points are indicated with their amplitudes $R_{\text{up,down}}$.

$$f_{\text{up}} = f_0 + 2\beta R_{\text{up}}^2 - \sqrt{(\beta R_{\text{up}}^2)^2 - \frac{1}{4}\Delta f^2} \text{ for } R_{\text{up}} \geq R_s \tag{1}$$
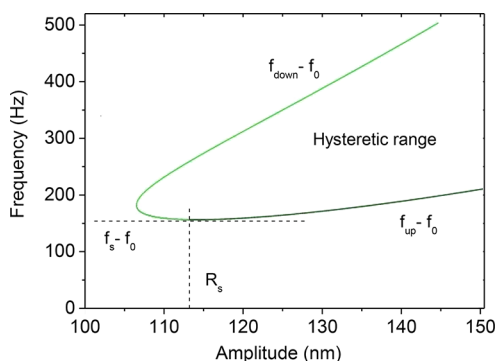
and

$$f_{\text{down}} = f_0 + 2\beta R_{\text{down}}^2 - \sqrt{(\beta R_{\text{down}}^2)^2 - \frac{1}{4}\Delta f^2}$$
$$\text{for } \frac{3^{1/4}}{\sqrt{2}} R_s < R_{\text{down}} \leq R_s \text{ (Case 1)}$$

$$f_{\text{down}} = f_0 + 2\beta R_{\text{down}}^2 + \sqrt{(\beta R_{\text{down}}^2)^2 - \frac{1}{4}\Delta f^2}$$
$$\text{for } R_{\text{down}} \geq \frac{3^{1/4}}{\sqrt{2}} R_s \text{ (Case 2)} \tag{2}$$

These functions are displayed in Figure 3. As we increase the driving force F_0, the maximum amplitude $R_{\max}$ linearly increases


Figure 3. Bifurcation branches. Calculated bifurcation frequencies from eqs 1 and 2 for the 250 μm device and magnetomotively loaded Q of 5000 (1 T field).

while the peak position shifts quadratically. The upper bifurcation point f_{up} then shifts monotonically toward higher frequencies, with a monotonically increasing amplitude R_{up} when F_0 is increased. On the other hand, the lower bifurcation point f_{down} has first an amplitude R_{down} that decreases (f_{down} being given by case 1 above), and then it increases again (f_{down} being then defined through case 2). At the spinodal point R_s,

$$f_{\text{up}} = f_{\text{down}} = f_s = f_0 + \frac{\sqrt{3}}{2}\Delta f.$$

The method we present builds on the work by Aldridge and Cleland:[30] the bifurcation positions are essentially *arbitrarily well-defined* (in the sense that in an ideal system only the thermal activation of the bifurcation process will limit the stability) and can be used for sensing/amplifying. We thus devise a technique enabling the characterization of frequency fluctuations themselves; indeed, the imprint of frequency fluctuations had been reported earlier in noise-induced bifurcation relaxation.[31] We show in Figure 4 histograms obtained on the f_{down} frequency position of the resonance of Figure 2. They are measured by ramping the frequency down from above f_{up} at constant speed and measuring the switching to the higher branch through a threshold detection. We repeat this protocol typically 1000 times to acquire enough statistics (see Figure 4 graph A left inset). The histogram obtained directly from the frequency time trace is then fit to a Gaussian (of standard deviation σ_f, graph A in Figure 4), while the power spectrum $S_f(f)$ of the fluctuations is also computed (defined as the FFT of the autocorrelation function). It displays a $1/f$-type structure (see Figure 4A right inset).

Some precautions have to be taken in order to ensure that the acquired data are unbiased: we first make sure that the bifurcation jump occurs within a single point of the acquisition trace (we thus have to lower the filtering time constant of the lock-in compared to Figure 2). Typically, we take one point every 40 ms with a frequency resolution typically 10 times smaller than the measured Gaussian spread. Second, we verify that we do not suffer from Brownian-type motion amplitude noise (at the mode frequency) that would activate relaxation of states when we are close enough to the bifurcation points.[30,31] Such activated bifurcation generates non-Gaussian and asymmetric statistics, which is ramping-speed dependent.[30] No such characteristics have been seen in our experiments: we first check that the ramping speed (of order 0.1−1 Hz/s) does not change the measured histogram, and second, we add a controlled amount of force noise (at the mechanical resonance) in order to see when relaxation is indeed noise-activated.[31] We see that a force noise equivalent to a bath temperature of about 10^6 K has to be reached in order to affect the frequency statistics. Note that 10^6 K is also the range of effective temperatures that are needed in order to see (asymmetric) frequency fluctuations transduced from Brownian motion through the Duffing nonlinearity.[17] Clearly, at 4.2 K with no added noise no such phenomena can occur. In the following,
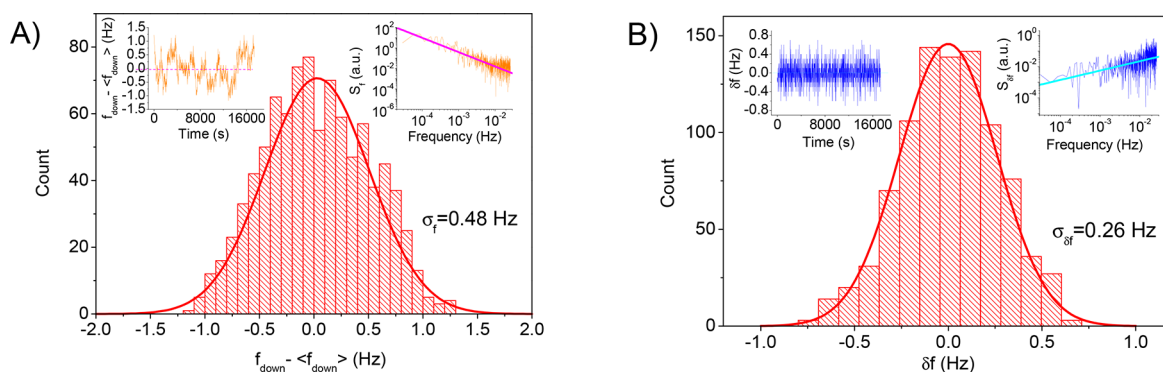
Figure 4. Statistics on frequency at low amplitudes. (A) Histogram obtained on the f_{down} relaxation point of Figure 2 (left inset: actual frequency time trace; right inset: power spectrum of the frequency fluctuations, displaying $1/f$-type structure). (B) Histogram obtained on the frequency jumps δf computed from the f_{down} time trace (left inset: δf time trace; right inset: power spectrum). The lines are Gaussian fits, and the power-law dependencies of the spectra are discussed in the text.

we make sure that no extra force noise is injected in the setup while measuring frequency fluctuations. Finally, the frequency drifts of our generators are characterized: we take two of them of the same type and measure the frequency stability of one against the timing of the other. Slow frequency fluctuations occur at the level of 1 mHz for 1 MHz signals over minutes, and 10 mHz for 10 MHz. This is at least 2 orders of magnitude smaller than what is seen here over the same periods of time and can be safely discarded.

We see that frequency fluctuations display a typical $1/f$-type behavior (right inset in Figure 4 A), as reported by others.[7,11] Indeed, the time trace has clearly some slowly drifting component (left inset in the same graph). This means that the statistics obtained *depend on the acquisition bandwidth*. For pure $1/f$ noise, the standard deviation σ_f (which is the square root of the power spectrum integral) depends on $\sqrt{\ln(f_{high}/f_{low})}$, with f_{high} the fastest frequency probed (defined from the time needed to acquire one bifurcation trace Δt_{min}, about 10 s) and f_{low} the lower frequency cutoff (set by the total acquisition time, about 3 h). In order to be as quantitative as possible, we look for an estimate of frequency noise, which is as independent from the protocol as possible. We therefore study the *frequency jumps* $\delta f(t) = f_{down}(t_{i+1}) - f_{down}(t_i)$ instead of $f_{down}(t)$; see Figure 4B left inset. The variance of this quantity $\sigma_{\delta f}^2$ is the well-known Allan variance,[32] computed for acquisition time $\Delta t_{min} = t_{i+1} - t_i$. Note that this quantity safely suppresses equipment low-frequency drifts (such as, besides the one characterized for the generator, temperature drifts due to the ^{4}He bath).

For a perfectly $1/f$ noise, the Allan variance at $\Delta t_{min} \to 0$ is independent[6] of f_{high} and f_{low} (see Methods). However, our power spectrum fits $S_0/f^{1+\epsilon}$ with $\epsilon \approx 0.4 \pm 0.2$. We calculate that over the most extreme settings that have been used, our Allan variance should not have changed by more than 50% (and in the data presented here by much less). Moreover, to prove that the $\Delta t_{min} \to 0$ assumption can be applied, we display in the right inset of Figure 4B the power spectrum $S_{\delta f}(f)$ of δf fluctuations: the data match the spectrum $\propto f$ directly computed from the fit of $S_f(f)$.

We can then compare the values of σ_f and $\sigma_{\delta f}$ that have been obtained. According to theory (see Methods) the first one should be about twice the second one in our conditions. This is indeed what we see in Figure 4, confirming that $\sigma_{\delta f}$ is a good quantitative measurement of frequency fluctuations. Besides,

the frequency stability defined as $\sigma_{\delta f}/f_0 \approx 0.3$ ppm falls within the expected range according to reported measured devices.[7] We thus demonstrate that our simple technique is functional: the key being that since the spectrum is $1/f$-type, we *do not need to be especially fast* to characterize frequency noise. With a phase locked loop setup one could measure fluctuations on much shorter time scales,[10] but our 10 s repetition rate is perfectly well adapted.

We now build on our method to thoroughly characterize frequency noise in SiN string devices. Let us apply this technique to the upper bifurcation point f_{up}. The method explained above is easily reversed in sweep direction and threshold detection. A similar time trace, spectrum, and histogram to Figure 4 obtained this way are shown in Figure 5. We see that the power spectrum displays the same $1/f^{1+\epsilon}$ law
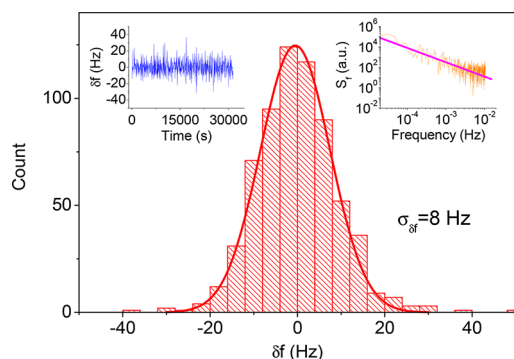

Figure 5. Large-amplitude statistics. Similar graphs to those in Figure 4 were obtained on the upper bifurcation point f_{up} (frequency jumps time trace in the left inset, power spectrum of frequency in the right inset, and histogram of δf in the main part of the graph). The line is a Gaussian fit, while the power spectrum follows $1/f^{1.4}$ (see text).

with $\epsilon \approx 0.4$. This is true for the complete study we realized on the same device and proves that different data sets can be consistently compared. The histogram is again Gaussian. But surprisingly, $\sigma_{\delta f}$ is now *much bigger* on the upper branch than on the lower one. We therefore make a complete study as a function of driving force (*i.e.*, motion amplitude). We discover that the standard deviation $\sigma_{\delta f}$ depends quadratically on motion amplitude R. Measuring at another magnetic field B_0, we find that it also depends linearly on the Q of the mechanical mode. However, measuring at different temperatures T_0 in the 1.4–30

K range, we realize that the small-amplitude value obtained is temperature-dependent, while the large-amplitude one is not.

This suggests the normalized plot of Figure 6, where the increase $\sigma_{\delta f}(T, R_{up,down})$ from the extrapolated $\sigma_{\delta f}(T, R_s)$ is
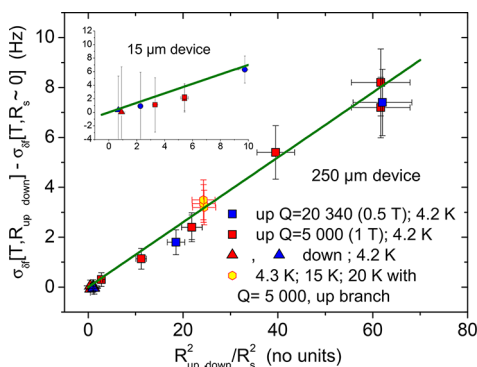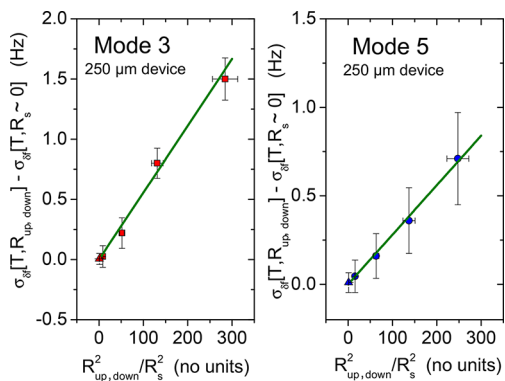

Figure 6. Universal plot for mode 1. Frequency noise increase *vs* squared amplitude normalized to the spinodal value R_s, for the first mode $n = 1$ of the 250 μm device. Various T_0 and B_0 (hence Q) have been used (see legend). Squares stand for upper branch bifurcation; triangles for lower. Inset: same result obtained with a 15 μm beam having $\beta = 1.1 \times 10^{19}$ Hz/m^2 (4.2 K and $Q = 17\,000$ red squares; 800 mK and $Q = 31\,000$ blue dots; the magnetomotive field broadening was negligible). The green line is a linear fit (see text).

plotted against the normalized variable $R_{up,down}^2/R_s^2$. The notation $R_s \approx 0$ means that the value is obtained from the linear fit, extrapolating at $R \to 0$. In order to verify the robustness of the result, we realize the same analysis with a similar device of 15 μm length. Some typical data are displayed in the inset of Figure 6. The noise properties obtained for this other device are very similar to the initial 250 μm long beam (but the quadratic dependence is different). However, the spectra better fit with $\epsilon \approx 0.2 \pm 0.2$.

We proceed with similar measurements performed on modes $n = 3$ and $n = 5$ of the 250 μm beam sample. All spectra display the same $1/f^{1.4}$ dependence as the $n = 1$ mode. The same normalized plots are displayed in Figure 7. However, this time the inferred quadratic dependencies are much weaker.

The nonlinear dependence of the frequency noise is rather unexpected; indeed, the nonlinear dephasing features observed for carbon-based devices[12] have not been reported for nitride

structures.[13] A possible source for such an effect could be a *purely intrinsic* property of the bifurcation effect itself. However, since our statistics could not be altered by reasonable changes in effective temperatures and frequency-sweep ramping speeds, such an explanation is improbable. If we then suppose the bifurcation process to be perfectly ideal, the nonlinear frequency noise observed should originate in *one of the parameters* defining the bifurcation frequencies. When the experiment is performed reasonably far from the spinodal point (which is always our case), we have

$$f_{up} \approx f_0 + \delta\phi(t) + \beta R_{up}^2 \qquad (3)$$

$$f_{down} \approx f_0 + \delta\phi(t) + 3\beta R_{down}^2 \qquad (4)$$

$$R_{up} \approx R_{max} \qquad (5)$$

$$R_{down} \approx \frac{1}{2^{2/3}}\left(\frac{R_{max}\Delta f}{\beta}\right)^{1/3} \qquad (6)$$

adapted from eqs 1 and 2, where we explicitly introduced the stochastic frequency variable $\delta\phi(t)$. For strings[26] $\beta \propto 1/(m_0 f_0)\left(\frac{E_Y A}{L^3}\right)$, the nonlinear frequency noise could be caused by (Gaussian) fluctuations of the Young's modulus $E_Y = E_0 + \delta E(t)$. However, to have the measured characteristics, this noise would have to be $\delta E/E_0 \propto 1/\Delta f$ and mode-dependent, which is difficult to justify: this explanation seems again unphysical.

The only possibility left is an *internal motional noise* with $R_{max} = R_{max_0} + \delta R$, leading to fluctuations $\propto \left(\frac{\delta R}{R_{max_0}}\right)\beta R_{max_0}^2$. The proper scalings, as reported in Figures 6 and 7, are thus only achieved by assuming *damping noise* $\delta\Gamma(t)$ with $\frac{\delta R}{R_{max_0}} = -\frac{\delta\Gamma}{\Delta f}$. As a result, it follows from eqs 3−6, $f_{up}(t) \approx f_0 + \delta\phi(t) + \beta R_{max_0}^2\left(1 - 2\frac{\delta\Gamma(t)}{\Delta f}\right)$, $f_{down}(t) \approx f_0 + \delta\phi(t) + \frac{3}{2^{4/3}}(\Delta f^2 \beta R_{max_0}^2)^{1/3}$ together with $f_s(t) = f_0 + \delta\phi(t) + \frac{\sqrt{3}}{2}\Delta f\left(1 + \frac{\delta\Gamma(t)}{\Delta f}\right)$. This means that both bifurcation frequencies suffer from frequency noise $\delta\phi$, while *only the upper branch* experiences damping fluctuations $\delta\Gamma$: they are *amplified* by the measurement method through a factor $\beta R_{max_0}^2/\Delta f$. Note that the frequency noise extrapolated at $R \to 0$ on the upper branch matches the one of the lower branch, but does not equal the one obtained at the spinodal point, simply because the expressions eqs 3−6 do not apply near R_s; this is emphasized through the writing $R_s \approx 0$ in our graphs.

The Allan deviation $\sigma_{\delta f}$ extrapolated to $R \to 0$ is thus characteristic of the frequency noise $\delta\phi$, while the slopes of the graphs in Figures 6 and 7 are $\frac{2}{\sqrt{3}}$ times the Allan deviation $\sigma_{\delta\Delta f}$ of the damping fluctuations. To our knowledge, the latter has not been reported in the literature so far. The mode parameters together with these 4.2 K frequency and damping noise figures are summarized in Table 1. $\sigma_{\delta\Delta f}$ is temperature-independent in the range studied, while $\sigma_{\delta f}^2$ is linear in T_0; this is displayed in Figure 8. The same temperature dependence of frequency noise has been reported in ref 11 (within an overall scaling factor) for a very similar device. In order to compare the various results,

Figure 7. Universal plot for modes 3 and 5. Normalized frequency noise plot for the same 250 μm device, for modes $n = 3$ (left) and $n = 5$ (right). The lines are linear fits (see text).

Table 1. Mode Parameters, Frequency, and Damping Fluctuations for Modes n = 1, 3, and 5 (250 μm Long Beam, 4.2 K)

mode number n	freq f_0	unloaded Q	duffing β	$\sigma_{\delta f}$ at $R_s \approx 0$	$\sigma_{\delta \Delta f}$ from $R_{up} \gg R_s$
$n = 1$	0.905 MHz	600 000 ± 10%	$8.5 \pm 0.5 \times 10^{15}$ Hz/m²	0.28 ± 0.05 Hz	0.11 Hz ± 10%
$n = 3$	2.68 MHz	450 000 ± 10%	$1.25 \pm 0.2 \times 10^{17}$ Hz/m²	0.1 ± 0.02 Hz	0.005 Hz ± 15%
$n = 5$	4.45 MHz	400 000 ± 20%	$5.7 \pm 0.5 \times 10^{17}$ Hz/m²	0.09 ± 0.02 Hz	0.0025 Hz ± 30%
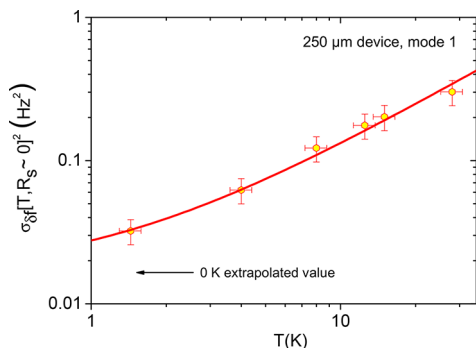
Figure 8. Temperature dependence of frequency fluctuations. Allan variance $\sigma_{\delta f}^2$ as a function of temperature (first mode of 250 μm device), as obtained for small motion $R \to R_s \approx 0$. The line is a linear fit, with the $T_0 = 0$ K extrapolated value emphasized by the arrow (see text). The variance of damping fluctuations $\sigma_{\delta \Delta f}^2$ is constant in the same range of temperatures.

values from the literature are presented in Table 2. We give the Allan deviation when it is reported; otherwise we list the direct frequency noise. The damping noise in the third line is recalculated from Figure IV.19 in ref 33.

We can only speculate on the microscopic mechanisms behind the reported features. The entities generating such noise are thought to be atomic-scale two-level systems, which could be defects or intrinsic to the materials in use.[6,11,20,33] A signature that also supports this view is the presence of *telegraph frequency noise* in many NEMS experiments (see, *e.g.*, ref 33). Ref 6 analyzed frequency noise in beams, *i.e.*, structures with no built-in stress. These authors assumed that thermally activated motion of a defect in a double-well potential from one minimum to the other caused a shift in the local Young's modulus. The motion of many such defects (following the mathematical arguments of ref 19) then causes a change in the average Young's modulus and consequently a change in the resonance frequency of the beam with power spectrum $\propto T/f$. The same argument was applied in ref 11 to analyze the frequency noise of string structures, where the built-in stress is large, even though the resonance frequency is nearly independent of the Young's modulus in the high-stress limit. We thus believe that it is more appropriate, in the interpretation of the present measurements on strings, to consider frequency fluctuations due to *stress fluctuations*. Indeed, point defects in crystals are characterized as elastic

dipoles that cause an orientation-dependent change in the strain (and consequently the stress) of a crystal.[34]

In our highest Q device, for the first flexure $n = 1$ frequency fluctuations at 4.2 K represent about 20% of the line width, and damping fluctuations about 5%. These parameters fall with mode number n (see Table 1), while both frequency f_0 and line width Δf increase. This means that the effect of fluctuations is *the strongest* on the first mode, but is usually difficult to visualize on standard frequency sweeps or time decay data; it is for instance expected that for a device rather equivalent to our 250 μm beam the measurements performed in ref 13 did not report any such features (see Methods).

CONCLUSION

In this article we present a very simple and reliable method to measure and characterize frequency noise in bistable resonators. The technique has been employed to describe thoroughly the intrinsic frequency noise of high-stress silicon-nitride doubly clamped beams. The measurements have been performed at low temperatures in a cryogenic vacuum, on two devices of very different lengths/fundamental resonance frequencies. The three first symmetric flexural modes of the longest beam have been studied.

We report on the Allan deviations of the frequency noise, presenting the same basic features as in refs 7 and 11: spectra of $1/f$-type, scaling linearly with temperature. The reported magnitudes of the noise $\delta f/f_0$ fall in the 0.5−0.01 ppm range, as expected for MHz devices.

We have also found unexpectedly *damping fluctuations*, which are amplified in the vicinity of bifurcation points. Our technique seems the most adapted for the detection and the quantification of such a noise process to date. We find that damping noise can be as large as about 5% of the total width of the resonance peak in our highest Q devices. It also sets a finite resolution attainable for the measurement of the frequency position of bifurcation points.

These features seem ubiquitous to all NEMS devices, and we do believe that damping noise and frequency noise originate in the same microscopic mechanism. But the latter remains elusive, and the most discussed candidate is based on two-level systems.[6,11] Because of the strength of the frequency noises reported here for high-stress devices, we propose that TLS are responsible for noise on the *stored stress* in the structure instead of the Young's modulus, as it was proposed in earlier papers discussing stress-free beams (*e.g.*, ref 6).

Table 2. Mode Parameters, Frequency, and Damping Fluctuations for Different Devices (Fundamental Flexure n = 1)[a]

device	freq f_0	Q	$\sigma_{\delta f}$ or σ_{f_0}	$\sigma_{\delta \Delta f}$
250 μm SiN/Al dc beam 4.2 K (this work)	0.905 MHz	600 000 ± 10%	0.28 ± 0.05 Hz	0.11 Hz ± 10%
15 μm SiN/Al dc beam 4.2 K (this work)	17.5 MHz	18 000 ± 10%	1.45 ± 0.1 Hz	0.6 Hz ± 10%
2 × 3 μm Si/Al goalpost 4.2 K, refs 31, 33	7.1 MHz	4700 ± 10%	1 ± 0.5 Hz on f_0	0.35 Hz ± 10%
380 μm SiN dc beam 5 K, ref 11	0.64 MHz	2 200 000	0.01 Hz on f_0	X
3.2 μm Si cantilever room temp, ref 7	45.2 MHz	6000	36 Hz	X

[a]The damping noise figure in the third line is recalculated from Figure IV.19 in ref 33.

Our technique can be easily adapted to any type of device, including MoS_2 and carbon-based systems in which nonlinear frequency noise has been reported.[12] We think that it should help advance the understanding of the underlying fundamental microscopic mechanisms that also significantly degrade the properties of existing NEMS devices and hinder their applicability.

METHODS

Device Fabrication. The structure was fabricated using e-beam lithography on a silicon substrate covered with a 100 nm SiN layer. The stochiometric nitride was grown using low-pressure chemical vapor deposition at the Cornell NanoScale Science & Technology Facility. It stores a biaxial stress of about 1 GPa. A 30 nm aluminum coating has been evaporated onto the sample in a Plassys e-gun machine. Its resistance at low temperature is about 1 $k\Omega$ for the 250 μm long device and 100 Ω for the 15 μm one. It served as a mask for the structure during the SF_6 reactive ion etching step used to pattern the SiN. The structure was then released using a final XeF_2 etching of the underlying silicon.

Measurements. The voltage drive was delivered by a Tektronix AFG3252 generator, through a 1 $k\Omega$ bias resistance, which created the drive current. The motion was actuated with the magnetomotive technique through a force $F(t) = I_0 \zeta L B_0 \cos(2\pi f t)$, which also leads to the detection of the velocity $\dot{x}(t)$ of the oscillation through a voltage $V(t) = \zeta L B_0 \dot{x}(t)$. ζ is a mode-dependent shape factor.[24] In the high-Q limit, the velocity in frequency domain is $i\omega_0 x(\omega)$ with $\omega_0 = 2\pi f_0$, hence an inverted definition for the signal quadratures X and Y with respect to displacement $x(t)$. Due to the symmetry of the scheme, only symmetric modes ($n = 1, 3, 5, ...$) can be addressed ($\zeta = 0$ otherwise). The magnetic field was generated with a small superconducting coil fed with a 10 A Kepco current source. The detected signal was processed with a Stanford SR 844 RF lock-in amplifier. Due to the finite impedance of the electric circuit seen by the NEMS (whose own characteristic impedance varies as $B_0{}^2$), the mechanical resonances are loaded by an additional damping $\propto B_0{}^2$. This provides the ability to tune the quality factors *in situ*.[24] Our calibration procedure is described in ref 25. It enables us to give all mechanical parameters in S.I. units (we thus quote X, Y in meters), while minimizing the loading effect. Loading is negligible for the 15 μm beam, but still large in the 250 μm device.

Spectra Mathematical Properties. Let us consider a frequency power spectrum for the stochastic resonance frequency $\omega_0 = 2\pi f_0$ of type $S_{\omega_0}(\omega) = A_0 / |\omega|^{1+\epsilon}$ (defined from $-\infty$ to $+\infty$). The variance can be defined from the integral of the spectrum, leading to $\sigma_{\omega_0}^2 = \frac{1}{2\pi} \int S_{\omega_0} d\omega = \frac{2A_0}{2\pi} \left[\frac{\omega_{low}^{-\epsilon} - \omega_{high}^{-\epsilon}}{\epsilon} \right]$ with ω_{low} and ω_{high} the lower and higher frequency cutoffs imposed by the experiment. For $\epsilon \to 0$ we have $\sigma_{\omega_0} \propto \sqrt{\ln[\omega_{high}/\omega_{low}]}$. Since $\delta\omega = \omega_0(t_{i+1}) - \omega_0(t_i) \approx \partial\omega_0(t)/\partial t \times \Delta t_{min}$ when $\Delta t_{min} \to 0$, we have $S_{\delta\omega}(\omega) \approx \Delta t_{min}^2 \omega^2 S_\omega(\omega)$. Thus, $\sigma_{\delta\omega}^2 \approx \frac{2A_0}{2\pi} \frac{(\Delta t_{min}\omega_{high})^2}{2} \left[\omega_{high}^{-\epsilon} \frac{1 - (\omega_{low}/\omega_{high})^{2-\epsilon}}{1 - \epsilon/2} \right]$. The Fourier transform imposes $\Delta t_{min}\omega_{high} \approx \pi$, and in the case $\epsilon \to 0$ we obtain $\sigma_{\delta\omega} \propto \sqrt{1 - (\omega_{low}/\omega_{high})^2}$, which is essentially independent of the cutoffs.[6] For $\epsilon \neq 0$, a small dependence on the bandwidth appears in the Allan variance $\sigma_{\delta\omega}^2$. For our acquisition bandwidths, this does not result in a too large scatter in data (within error bars).

Impact on Frequency-Domain and Time-Domain Measures. With a noise of type $S_{\omega_0}(\omega) = A_0 / |\omega|^{1+\epsilon}$, we can take as an estimate of the relevant fluctuations time scale $\tau_c^{-1} \approx \omega_{low}/\pi$: the weight is at the lowest accessible frequencies. We thus always verify $\sigma_{\omega_0}\tau_c \gg 1$, which means that the phase diffusion of the mechanical mode is in the inhomogeneous broadening limit, in analogy with nuclear magnetic resonance.[13,16,17] In the frequency domain, the response $\chi_{meas}(\omega)$ is the convolution of the standard (complex-valued, defining the two quadratures) susceptibility $\chi(\omega)$ with the (Gaussian) distribution of

frequencies $p(\delta\varphi) = 1/\sqrt{2\pi\sigma_{\omega_0}^2} \exp\left(-\frac{1}{2}\delta\varphi^2/\sigma_{\omega_0}^2\right)$, with $\delta\varphi = 2\pi\delta\phi$ in rad/s. This means that at each scanned frequency ω the measurement is performed over a long enough time scale such that all fluctuations are explored. On the other hand, the small damping fluctuations are simply filtered out by the acquisition setup (here, a lock-in amplifier): they have no relevant impact on the resonance peak measured, even at very large motion amplitudes. We conclude that only frequency noise will contribute to the definition of a T_2, the decoherence time involving relaxation T_1 and dephasing σ_{ω_0}.[13] In the time domain, in the linear regime the complex susceptibility $\bar{\chi}_{meas}(t)$ (*i.e.*, decay of the two quadratures) is simply the Fourier transform (FT) of $\chi_{meas}(\omega)$. It can also be written $\bar{\chi}_{meas}(t) = \langle \exp(i\delta\varphi t) \rangle \bar{\chi}(t)$ with $\bar{\chi}(t)$ the FT of $\chi(\omega)$ and $\langle \exp(i\delta\varphi t) \rangle = \exp\left(-\frac{1}{2}\sigma_{\omega_0}^2 t^2\right)$ the average over frequency fluctuations. In the nonlinear regime, the average decay of the two quadratures is written as

$$\bar{\chi}_{meas}(t) = \langle \exp(i\delta\varphi t) \rangle \left\langle \exp\left(-i2\frac{\beta R_{max_0}^2}{\Delta\omega}\delta\gamma t\kappa[t]\right) \right\rangle \bar{\chi}(t)$$

with $\kappa[t] = \frac{1 - \exp[-t\Delta\omega]}{t\Delta\omega}$ and $\bar{\chi}(t)$ defined in ref 28, the second average being over damping fluctuations $\delta\gamma = 2\pi\delta\Gamma$; we write $\Delta\omega = 2\pi\Delta f$ in rad/s. The function κ is characteristic of the decay of the nonlinear frequency pulling due to the Duffing term,[28] $\propto R_{max_0}^2$. In practice, this assumes that both quadratures are measured independently, averaging many decay traces starting from the same (noisy) $t = 0$ amplitude R_{max_0} imprinted by the slow fluctuations of damping $\delta\gamma$. The second average can be explicitly calculated:

$$\left\langle \exp\left(-i2\frac{\beta R_{max_0}^2}{\Delta\omega}\delta\gamma t\kappa[t]\right) \right\rangle = \exp\left[-\frac{1}{2}\left(2\frac{\beta R_{max_0}^2}{\Delta\omega}\right)^2 \sigma_{\delta\Delta\omega}^2(t\kappa[t])^2\right].$$

In the time domain, the impact of damping fluctuations (of variance $\sigma_{\delta\Delta\omega}^2$) is thus *amplified* by the same term as in the bifurcation measurement: $\frac{\beta R_{max_0}^2}{\Delta\omega}$. However, to have a measurable effect (within experimental error bars) both amplitude R_{max_0} and fluctuations $\sigma_{\delta\Delta\omega}$ have to be very large; in experiments of the type of ref 13 based on devices similar to our 250 μm, no such effect has been reported. Measuring the decay of the two quadratures leads then to the definition of $\bar{T}_2$, roughly equivalent to T_2.[13] Note that the decay of the motion amplitude $|\bar{\chi}(t)|^2$ remains unaffected by frequency and damping noise, leading to the proper T_1 definition.[13]

AUTHOR INFORMATION

Corresponding Author
*E-mail: eddy.collin@neel.cnrs.fr. Phone: +33 4 76 88 78 31.

ORCID
Eddy Collin: 0000-0002-4460-5656

Present Address
#Institut d'Electronique, de Microélectronique et de Nanotechnologie (IEMN), Université Lille & CNRS, 59000 Lille, France.

Notes
The authors declare no competing financial interest.

REFERENCES

(1) Moser, J.; Güttinger, J.; Eichler, A.; Esplandiu, M. J.; Liu, D. E.; Dykman, M. I.; Bachtold, A. Ultrasensitive Force Detection with a Nanotube Mechanical Resonator. *Nat. Nanotechnol.* **2013**, *8*, 493−496.

(2) Li, M.; Tang, H. X.; Roukes, M. L. Ultra-sensitive NEMS-based Cantilevers for Sensing, Scanned Probe and Very High-frequency Applications. *Nat. Nanotechnol.* **2007**, *2*, 114−120.

(3) Rugar, D.; Budakian, R.; Mamin, H. J.; Chui, B. W. Single Spin Detection by Magnetic Resonance Force Microscopy. *Nature* **2004**, *430*, 329−332.

(4) Chaste, J.; Eichler, A.; Moser, J.; Ceballos, G.; Rurali, R.; Bachtold, A. A Nanomechanical Mass Sensor with Yoctogram Resolution. *Nat. Nanotechnol.* **2012**, *7*, 301−304.

(5) Pirkkalainen, J.-M.; Cho, S. U.; Li, J.; Paraoanu, G. S.; Hakonen, P. J.; Sillanpää, M. A. Hybrid Circuit Cavity Quantum Electrodynamics with a Micromechanical Resonator. *Nature* **2013**, *494*, 211−215.

(6) Cleland, A. N.; Roukes, M. L. Noise Processes in Nanomechanical Resonators. *J. Appl. Phys.* **2002**, *92*, 2758−2769.

(7) Sansa, M.; Sage, E.; Bullard, E. C.; Gély, M.; Alava, T.; Colinet, E.; Naik, A. K.; Villanueva, L. G.; Duraffourg, L.; Roukes, M. L.; Jourdan, G.; Hentz, S. Frequency Fluctuations in Silicon Nano-resonators. *Nat. Nanotechnol.* **2016**, *11*, 552−558.

(8) Zhang, Y.; Moser, J.; Güttinger, J.; Bachtold, A.; Dykman, M. I. Interplay of Driving and Frequency Noise in the Spectra of Vibrational Systems. *Phys. Rev. Lett.* **2014**, *113*, 255502.

(9) Greywall, D. S.; Yurke, B.; Busch, P. A.; Pargellis, A. N.; Willett, R. L. Evading Amplifier Noise in Nonlinear Oscillators. *Phys. Rev. Lett.* **1994**, *72*, 2992−2995.

(10) Feng, X. L.; He, R. R.; Yang, P. D.; Roukes, M. L. Phase Noise and Frequency Stability of Very-High Frequency Silicon Nanowire Nanomechanical Resonators. *Transducers Eurosens. XXVII, Int. Conf. Solid-State Sens., Actuators Microsyst., 17th* **2007**, 327−330.

(11) Fong, K. Y.; Pernice, W. H. P.; Tang, H. X. Frequency and Phase Noise of Ultrahigh Q Silicon Nitride Nanomechanical Resonators. *Phys. Rev. B: Condens. Matter Mater. Phys.* **2012**, *85*, 161410R.

(12) Schneider, B. H.; Singh, V.; Venstra, W. J.; Meerwaldt, H. B.; Steele, G. A. Observation of Decoherence in a Carbon Nanotube Mechanical Resonator. *Nat. Commun.* **2014**, *5*, 5819.

(13) Maillet, O.; Vavrek, F.; Fefferman, A. D.; Bourgeois, O.; Collin, E. Classical Decoherence in a Nanomechanical Resonator. *New J. Phys.* **2016**, *18*, 073022.

(14) Atalaya, J.; Isacsson, A.; Dykman, M. I. Diffusion-induced Dephasing in Nanomechanical Resonators. *Phys. Rev. B: Condens. Matter Mater. Phys.* **2011**, *83*, 045419.

(15) Yang, Y. T.; Callegari, C.; Feng, X. L.; Roukes, M. L. Surface Adsorbate Fluctuations and Noise in Nanoelectromechanical Systems. *Nano Lett.* **2011**, *11*, 1753−1759.

(16) Zhang, Y.; Dykman, M. I. Spectral Effects of Dispersive Mode Coupling in Driven Mesoscopic Systems. *Phys. Rev. B: Condens. Matter Mater. Phys.* **2015**, *92*, 165419.

(17) Maillet, O.; Zhou, X.; Gazizulin, R. R.; Maldonado Cid, A. I.; Defoort, M.; Bourgeois, O.; Collin, E. Nonlinear Frequency Transduction of Nanomechanical Brownian Motion. *Phys. Rev. B: Condens. Matter Mater. Phys.* **2017**, *96*, 165434.

(18) Atalaya, J.; Kenny, T. W.; Roukes, M. L.; Dykman, M. I. Nonlinear Damping and Dephasing in Nanomechanical Systems. *Phys. Rev. B: Condens. Matter Mater. Phys.* **2016**, *94*, 195440.

(19) Dutta, P.; Horn, P. M. Low-frequency Fluctuations in Solids: 1/f Noise. *Rev. Mod. Phys.* **1981**, *53*, 497−516.

(20) Behunin, R. O.; Intravaia, F.; Rakich, P. T. Dimensional Transformation of Defect-induced Noise, Dissipation, and Non-linearity. *Phys. Rev. B: Condens. Matter Mater. Phys.* **2016**, *93*, 224110.

(21) Hoehne, F.; Pashkin, Y. A.; Astafiev, O.; Faoro, L.; Ioffe, L. B.; Nakamura, Y.; Tsai, J. S. Damping in High-frequency Metallic Nanomechanical Resonators. *Phys. Rev. B: Condens. Matter Mater. Phys.* **2010**, *81*, 184112.

(22) Venkatesan, A.; Lulla, K. J.; Patton, M. J.; Armour, A. D.; Mellor, C. J.; Owers-Bradley, J. R. Dissipation Due to Tunneling Two-level Systems in Gold Nanomechancial Resonators. *Phys. Rev. B: Condens. Matter Mater. Phys.* **2010**, *81*, 073410.

(23) Miao, T.; Yeom, S.; Wang, P.; Standley, B.; Bockrath, M. Graphene Nanoelectromechanical Systems as Stochastic-Frequency Oscillators. *Nano Lett.* **2014**, *14*, 2982−2987.

(24) Cleland, A. N.; Roukes, M. L. External Control of Dissipation in a Nanometer-scale Radiofrequency Mechanical Resonator. *Sens. Actuators, A* **1999**, *72*, 256−261.

(25) Collin, E.; Defoort, M.; Lulla, K.; Moutonet, T.; Heron, J.-S.; Bourgeois, O.; Bunkov, Y. M.; Godfrin, H. *In situ* Comprehensive Calibration of a Tri-port Nano-electro-mechanical Device. *Rev. Sci. Instrum.* **2012**, *83*, 045005.

(26) Lifshitz, R.; Cross, M. C. Nonlinear Dynamics of Nano-mechanical and Micromechanical Resonators. In *Reviews of Nonlinear Dynamics and Complexity*; Schuster, H. G., Ed.; Wiley: VCH, 2008; pp 1−52.

(27) Matheny, M. H.; Villanueva, L. G.; Karabalin, R. B.; Sader, J. E.; Roukes, M. L. Nonlinear Mode-Coupling in Nanomechanical Systems. *Nano Lett.* **2013**, *13*, 1622−1626.

(28) Collin, E.; Bunkov, Y. M.; Godfrin, H. Addressing Geometric Nonlinearities with Cantilever Microelectromechanical Systems:Beyond the Duffing Model. *Phys. Rev. B: Condens. Matter Mater. Phys.* **2010**, *82*, 235416.

(29) Landau, L. D.; Lifshitz, E. M. In *Mechanics*; Elsevier: New York, 1976.

(30) Aldridge, J. S.; Cleland, A. N. Noise-enabled Precision Measurements of a Duffing Nanomechanical Resonator. *Phys. Rev. Lett.* **2005**, *94*, 156403.

(31) Defoort, M.; Puller, V.; Bourgeois, O.; Pistolesi, F.; Collin, E. Scaling Laws for the Bifurcation Escape Rate in a Nanomechanical Resonator. *Phys. Rev. E* **2015**, *92*, 050903R.

(32) Allan, D. W. Time And Frequency (Time-Domain) Character-ization, Estimation, and Prediction of Precision Clocks and Oscillators. *IEEE Trans. Ultrason. Eng.* **1987**, *34*, 647−654.

(33) Defoort, M. In *Non-linear dynamics in nano-electromechanical systems at low temperatures*; Ph.D. Thesis, Université Grenoble Alpes, 2014.

(34) Nowick, A.; Berry, B. In *Anelastic Relaxation in Crystalline Solids*; Academic Press: New York, 1972.